

Higher order contribution to the propagation characteristics of low frequency transverse waves in a dusty plasma

A P MISRA¹, A ROY CHOWDHURY¹ and S N PAUL²

¹High Energy Physics Division, Department of Physics, Jadavpur University, Kolkata 700 032, India

²Faculty of Science, Serampore Girls' College, Hoogly 712 201, India
E-mail: arcphy@cal2.vsnl.net.in; sailenpaul@rediffmail.com

MS received 15 April 2003; revised 23 March 2004; accepted 5 May 2004

Abstract. Characteristic features of low frequency transverse wave propagating in a magnetised dusty plasma have been analysed considering the effect of dust-charge fluctuation. The distinctive behaviours of both the left circularly polarised and right circularly polarised waves have been exhibited through the analysis of linear and non-linear dispersion relations. The phase velocity, group velocity, and group travel time for the waves have been obtained and their propagation characteristics have been shown graphically with the variations of wave frequency, dust density and amplitude of the wave. The change in non-linear wave number shift and Faraday rotation angle have also been exhibited with respect to the plasma parameters. It is observed that the effects of dust particles are significant only when the higher order contributions are considered. This may be referred to as the 'dust regime' in plasma.

Keywords. Dust plasma; transverse wave; group travel time; Faraday rotation angle; non-linear wave number shift.

PACS No. 52.35.-g

1. Introduction

Non-linear interaction of waves in plasma and in the ionosphere exhibits many important and fascinating characteristics of dispersive waves [1–4]. Of late, a new scenario has emerged in Plasma Physics due to the importance of dusty plasma. The relevance of dusty plasma in ionosphere, planetary rings, cometary tails, asteroid zones as well as in laboratory plasmas are now well-recognised. In contrast to the ordinary plasmas, dusty plasmas contain an additional species of large dust sized dust grains of radii in the range of 10^{-2} – 10^{-6} cm, which in most situations are found to be negatively charged. The presence of these massive and highly charged particles can significantly change the collective behaviour of plasma [5–7]. In laboratory plasmas, dust particles appear as impurities in magnetohydrodynamic

(MHD) generators, high z-impurities from the walls of Tokamaks [8,9]. Due to the heavy mass of the dust particles the time of response of dust grains to high frequency oscillations is very large. In fact they give rise to low frequency modes such as ‘dust acoustic wave’, ‘dust-ion acoustic wave’. Moreover, the charge fluctuations of the dust grains give rise to interesting characteristics of dust acoustic waves [10–12].

It is worthwhile to mention that the experimental observations on dust-acoustic wave in dust charged plasma have been made by Barkman *et al* [13] supporting the theoretical observations of Rao *et al* [6]. From the self-consistent equations for ion density, envelope electric field and charge variations of dust particles in the plasma, several authors [14] investigated modulational instability of Langmuir waves related to dust charging process. It is interesting to note that the propagation of surface waves on the interface of semi-infinite dusty plasma is significantly modified by the fluctuating charge of dust particles [15]. Paul *et al* [16] showed that the streaming motion and attachment coefficient for charging the dust particles have important role on the formation of solitary waves in dusty plasma. Recently, Burman *et al* [17] investigated the propagation of both low and high frequency waves in a dusty plasma in the presence of positrons and generalised the results of the previous authors regarding the characteristics of dust acoustic waves. Moreover, they found that non-linear localisation of high frequency electromagnetic field in such a plasma generates magnetic field. More recently, Mondal *et al* [18] showed that pseudopotential in a dusty plasma has a positive and inverted profile which prevents trapping of particles and does not favour the formation of solitary waves in a bounded dusty plasma. However, propagation of low frequency waves in dusty plasma, particularly considering the non-linear effects, has not yet been studied by any of the previous authors. So in the present paper we have tried to exhibit the wave characteristics like phase velocity, group velocity etc. for low frequency transverse waves in the presence of charge fluctuations. In conformity with the usual expectations it is seen that the charge fluctuations affect only the non-linear modes, while the left circularly polarised (LCP) and right circularly polarised (RCP) modes behave quite differently. The existence of cut-off frequency is displayed in the various resonance zones. Lastly we have calculated the group travel time, Faraday rotation angle and wave number shift with the variation of frequency, amplitude and density inside the plasma. The results have been graphically shown by considering the plasma parameters in dusty plasma of the Saturn E-ring and other astrophysical objects.

2. Formulation

We consider a plasma consisting of electrons, singly charged ions and negatively charged dust grains. We further assume that a hydrodynamic description is possible, and due to the continuous collisions of the dust grains with the stream of electrons and ions, the net charge on a dust particle varies. The equations describing the plasma can be written as follows:

$$\frac{\partial n_s}{\partial t} + \nabla \cdot (n_s \vec{v}_s) = -\beta_s n_s, \quad (1)$$

$$\frac{\partial \vec{v}_s}{\partial t} + (\vec{v}_s \cdot \nabla) \vec{v}_s = \frac{Q_s}{m_s} \left(\vec{E} + \frac{1}{c} \vec{v}_s \times \vec{B} \right) - \beta_s \vec{v}_s, \quad (2)$$

$$\nabla \times \vec{E} = -\frac{1}{c} \frac{\partial \vec{B}}{\partial t}, \quad (3)$$

$$\nabla \times \vec{B} = \frac{1}{c} \frac{\partial \vec{E}}{\partial t} + \frac{4\pi}{c} \sum_s Q_s n_s \vec{v}_s, \quad (4)$$

$$\nabla \cdot \vec{E} = 4\pi \sum_s Q_s n_s, \quad (5)$$

$$\nabla \cdot \vec{B} = 0, \quad (6)$$

where 's' stands for i, e, d denoting respectively the ion, electron and dust; $Q_i = e$, $Q_e = -e$ and $Q_d = -q_d$ with $q_d > 0$ is the charge on the dust grain. Also, n_s and v_s denote respectively the density and velocity of the s-species particle. Moreover, \vec{E} and \vec{B} respectively stand for electric and magnetic field. In eqs (1) and (2), β_e and β_i represent the attachment frequencies of electrons and ions to the dust grains, so that the right side of eq. (1) describes the losses in the electron and ion densities.

As the charging process in magnetised dusty plasma is not yet fully examined, we assume that the fluctuation of charge of dust particles due to electron current and ion current into dust particles over corresponding equilibrium values I_{e0}, I_{i0} as [19,20]

$$I_e = -\pi r^2 e \sqrt{\frac{8KT_e}{\pi m_e}} n_e \exp\left[\frac{e(\phi_f - \phi_p)}{KT_e}\right], \quad (7)$$

$$I_i = \pi r^2 e \sqrt{\frac{8KT_i}{\pi m_i}} n_i \exp\left[1 - \frac{e(\phi_f - \phi_p)}{KT_i}\right], \quad (8)$$

where r is the radius of the grain, K the Boltzmann constant, $\phi_f - \phi_p$ the difference between the grain potential and the plasma potential, and T_e, T_i stand for electron and ion temperature respectively.

The dust charge fluctuation due to electron and ion currents is governed by the equation

$$\frac{dq_d}{dt} = I_e + I_i, \quad (9)$$

where I_e and I_i are given by (7) and (8).

To derive the dispersion relation in the dust regime, we set

$$n_s = n_s^{(0)} + \epsilon n_s^{(1)} + \epsilon^2 n_s^{(2)} + \dots$$

$$\vec{v}_s = \epsilon \vec{v}_s^{(1)} + \epsilon^2 \vec{v}_s^{(2)} + \dots$$

$$q_d = -q_d^{(0)} + \epsilon q_d^{(1)} + \epsilon^2 q_d^{(2)} + \dots$$

$$\vec{E} = \epsilon \vec{E}^{(1)} + \epsilon^2 \vec{E}^{(2)} + \dots$$

$$\vec{B} = \vec{B}^{(0)} + \epsilon \vec{B}^{(1)} + \epsilon^2 \vec{B}^{(2)} + \dots \quad (10)$$

where the superscripts 0, 1, 2 etc. stand for the order of perturbations and $q_d^0 > 0$. The forms of the LCP and RCP waves are assumed to be

$$E_{\pm}^{(1)} = a(e^{i\theta_{\pm}} + e^{-i\theta_{\mp}}), \quad (11)$$

where a represents the constant amplitude of the wave and

$$\theta_{\pm} = (k_{\pm}z - \omega t),$$

$$E_{\pm}^{(1)} = E_x^{(1)} \pm iE_y^{(1)}.$$

The subscripts with a + and – sign represent the LCP and RCP waves respectively. K and ω represent the wave number and frequency of the wave.

Using (10) in eqs (7) and (8) we have the perturbed electron and ion currents into the dust grain over corresponding equilibrium values $I_e^{(0)}, I_i^{(0)}$ as

$$I_e^{(1)} = -|I_e^{(0)}| \left(\frac{n_e^{(1)}}{n_e^{(0)}} + \frac{e\phi_f^{(1)}}{KT_e} \right), \quad (12)$$

$$I_i^{(1)} = -|I_i^{(0)}| \left(\frac{n_i^{(1)}}{n_i^{(0)}} - \frac{e\phi_f^{(1)}}{\omega_i^{(0)}} \right), \quad (13)$$

where

$$I_s^{(0)} = \pi r^2 e \sqrt{\left(\frac{8KT_s}{\pi m_s} \right)} \left(\frac{n_s^{(0)}}{KT_s} \right) \omega_s^{(0)}; \quad s = e, i \quad (14)$$

$$\omega_s^{(0)} = KT_s + Q_s \phi_f^{(0)} \quad (15)$$

and $\phi_f^{(1)}$ is the fluctuation in the dust grain potential given by $\phi_f^{(1)} = q_d^{(1)}/C$, C being the capacitance of the dust grain and $\omega_s^{(0)}$ the equilibrium floating potential. Substitution of (12) and (13) into (9) give

$$\frac{dq_d^{(1)}}{dt} + \eta q_d^{(1)} = |I_e^{(0)}| \left(\frac{n_i^{(1)}}{n_i^{(0)}} - \frac{n_e^{(1)}}{n_e^{(0)}} \right), \quad (16)$$

$$\frac{dq_d^{(2)}}{dt} + \zeta q_d^{(2)} = |I_e^{(0)}| \left(\frac{n_i^{(2)}}{n_i^{(0)}} - \frac{n_e^{(2)}}{n_e^{(0)}} \right), \quad (17)$$

where

$$\eta = \frac{e|I_e^{(0)}|}{C} \left(\frac{1}{KT_e} + \frac{1}{\omega_i^{(0)}} \right),$$

$$\zeta = \frac{e|I_e^{(0)}|}{C} \left(\frac{1}{\omega_e^{(0)}} + \frac{1}{\omega_i^{(0)}} \right),$$

and $I_e^{(0)} + I_i^{(0)} = 0$ in equilibrium.

Using (10)–(17) in (1)–(6) we obtain the first-order and third-order dispersion relations correct up to first harmonic part given by

$$\frac{c^2 k_{\pm}^2}{\omega^2} = 1 - \frac{\omega_e^2}{\omega(\omega \pm \Omega_e + i\beta_e)} - \frac{\omega_i^2}{\omega(\omega \mp \Omega_i + i\beta_i)} - \frac{\omega_d^2}{\omega(\omega \pm \Omega_d)} \quad (18)$$

and

$$\begin{aligned} \frac{c^2 k_{\pm}^2}{\omega^2} = & 1 - \frac{\omega_e^2}{\omega(\omega \pm \Omega_e + i\beta_e)} - \frac{\omega_i^2}{\omega(\omega \mp \Omega_i + i\beta_i)} - \frac{\omega_d^2}{\omega(\omega \pm \Omega_d)}, \\ & - \frac{\alpha_i^2}{N\omega^2} \Lambda_1 \eta_1 - \frac{\alpha_e^2}{N\omega^2} \Lambda_2 \eta_2 - \frac{\alpha_d^2}{N\omega^2} \Lambda_3 \eta_3, \end{aligned} \quad (19)$$

where

$$\omega_s = \sqrt{\frac{4\pi n_s^{(0)} e^2}{m_s}}, \quad \omega_d = \sqrt{\frac{4\pi n_d^{(0)} q_d^{(0)2}}{m_d}}; \quad s = e, i$$

being respectively the plasma frequencies for electron, ion and dust grains respectively and $\alpha_s = a q_s^{(0)} / m_s \omega c$, $s = i, e, d$ and $q_{e,i}^{(0)} = e$ and $\Lambda_s, \eta_s, s = 1, 2, 3$ are functions of $\omega, \omega_s, \Omega_s, \beta_s, k_{\pm}, \zeta$ etc. In the derivations of eqs (18) and (19) we have assumed that $E_z^{(1)} = B_z^{(1)} = v_{sz}^{(1)} = 0$; $E_{\pm}^{(2)} = v_{s\pm}^{(2)} = B_{\pm}^{(2)} = B_z^{(2)} = 0$, where $E_{\pm}^{(2)} = E_x^{(2)} \pm iE_y^{(2)}$ etc. The terms on the right side of eq. (19) which are proportional to α_s ($s = e, i, d$) and which depend on the plasma and dust gyro frequency as well as the attachment frequencies are due to the non-linear effects in the plasma.

3. Results and discussions

A. Dispersion relations

We are now interested in the special one when $\omega \approx \Omega_d, \omega \ll \Omega_i, \Omega_e$ and then the linear dispersion relations (18) take the form

$$\frac{c^2 k_{\pm}^2}{\omega^2} = 1 - \frac{\omega_d^2}{\omega(\omega \pm \Omega_d)}. \quad (20)$$

From (20) it is very clear that the LCP component of waves never resonates except at $\omega = 0$ or $\Omega_d = 0$ which are physically impossible in a magnetised plasma, whereas the RCP component resonates with negatively charged dust grains at $\omega = \Omega_d$. The dispersion diagram for the LCP wave is shown in figure 1 using the same scale. From the figure it is clear that the linear LCP wave is more dispersive than the non-linear one.

On the other hand when $\omega \approx \Omega_d$ the non-linear dispersion relations (19) lead to

$$n_L^2 \equiv \frac{c^2 k_{r+}^2}{\omega^2} \approx \frac{X(A_1 + \sqrt{A_1^2 + B_1^2})}{2A_1(\Delta\omega)} \left(1 - \frac{4\Omega_d^2}{3\omega_d(\Delta\omega)}\right), \quad (21)$$

$$n_R^2 \equiv \frac{c^2 k_{r-}^2}{\omega^2} \approx \frac{(-A_1 + \sqrt{A_1^2 + B_1^2})}{A_1(\Delta\omega)} \left[\frac{A_1\omega_d^2}{\Omega_d\sqrt{A_1^2 + B_1^2}} + 2X \left(1 - \frac{2\Omega_d^2}{3\omega_d(\Delta\omega)}\right) \right], \quad (22)$$

where

$$X = \frac{3A_1\omega_d^4\alpha_e^2(2\Omega_d + 3\omega_d)}{16\Omega_d(N_1^2 + N_2^2)(\zeta^2 + 4\Omega_d^2)\gamma_1},$$

$$N_1 = \text{Re } N = (2/\Omega_d)(\omega_d^2 - 4\Omega_d^2)(4\Omega_d^2 - \beta_e\beta_i) + 2\Omega_d(\omega_i^2 - 4\omega_e^2)$$

$$N_2 = \text{Im } N = 4(\omega_d^2 - 4\Omega_d^2)(\beta_e + \beta_i) + \beta_e\omega_i^2 - 4\beta_i\omega_e^2,$$

$$A_1 = (\zeta V_1 - 4\Omega_d^2 V_2)N_1 + 2\Omega_d(V_1 + \zeta V_2)N_2$$

$$B_1 = -(\zeta V_1 - 4\Omega_d^2 V_2)N_2 + 2\Omega_d(V_1 + \zeta V_2)N_1,$$

$$V_1 = (4\Omega_d^2 + \beta_e\beta_i) \left(\frac{\gamma_5}{4\Omega_d^2 + \beta_i^2} + \frac{\gamma_3}{4\Omega_d^2 + \beta_e^2} \right)$$

$$V_2 = (\beta_e - \beta_i) \left(\frac{\gamma_5}{4\Omega_d^2 + \beta_i^2} - \frac{\gamma_3}{4\Omega_d^2 + \beta_e^2} \right), \gamma_3 = \frac{m_e^2 m_i}{e^3}, \gamma_5 = \frac{m_i^2 m_e}{e^3},$$

where n_L and n_R respectively denote the non-linear refractive indices and $\Delta\omega = \Omega_d - \omega$. Note that here we have made use of the linear approximations

$$ck_+ \approx \omega, \quad ck_- \approx \omega_d \sqrt{\frac{\omega}{\Omega_d}} \left(1 + \frac{\omega}{2\Omega_d}\right).$$

In (21) and (22) the subscript 'r' in k denotes the real part and $\Delta\omega = \Omega_d - \omega$. The dispersion diagrams for both LCP and RCP waves are presented in figures 2a-2c with respect to ω with the variations of amp. of the electric field and density inside the plasma. The numerical data taken in CGS units are those used by Tsytovich *et al* [21] and Horayani [22] in Saturn's E-ring as: $n_d^{(0)} = 10^{-16} \text{ cm}^{-3}$, $n_i^{(0)} = 2 \times 10 \text{ cm}^{-3}$, $n_e^{(0)} = 10 \text{ cm}^{-3}$, $B_0 = 2.1 \times 10^{-1} \text{ G}$, $|\vec{E}| = 0.8 \times 10^{-4} \text{ stat volt/cm}$, $q_d^{(0)} = 4.8 \times 10^7 \text{ stat coulomb}$, $m_d = 1.67 \times 10^{-3} \text{ g}$, $\omega \sim 10^{-1} \text{ rad/s}$, $\zeta = 1.31 \times 10^{-1}$, $|I_e^{(0)}| = 1.3 \times 10^8 \text{ stat amp/cm}^2$.

In figure 1 the dispersion diagrams for linear and non-linear RCP waves have been compared to show that non-linear wave has larger refractive index than the linear one.

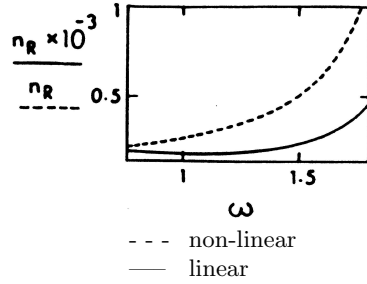


Figure 1. Propagation of linear and non-linear RCP waves: variation of n_R with frequency ω .

Figures 2a and 2b show the nature of propagation of the LCP component of waves with the variation of densities inside the plasma and intensity of the electric field. Numerical estimation shows that the LCP wave can propagate only in the region $0 < \omega < 1.972$ and cannot propagate for $\omega > 1.972$.

On the other hand the RCP component of waves can propagate only in $0 < \omega < 1.99$ and cannot propagate for $\omega > 1.99$. The propagation behaviours of RCP waves with variations of densities are shown in figure 2c.

B. Phase velocity

The phase velocity of the linear RCP wave obtained from (20) is

$$\left(\frac{\omega}{k_-}\right) = \frac{c\sqrt{1 - \frac{\Omega_d}{\omega}}}{\sqrt{1 - \frac{\Omega_d}{\omega} - \frac{\omega_d^2}{\omega^2}}} \quad (23)$$

which shows that the RCP wave can propagate in two frequency domains $0 < \omega < \Omega_d$ and $\omega > \Omega_d + \frac{\omega_d^2}{\Omega_d}$. The details of phase velocity, group velocity and dispersion diagrams for linear RCP wave have already been studied by Sarkar *et al* [23], and so we do not represent them here.

In the case of non-linear LCP and RCP waves, the corresponding phase velocities from eqs (21) and (22) are given by the expressions

$$v_{\phi+} \approx c\sqrt{\frac{2\Delta\omega}{X}} \left[\frac{A_1 + \sqrt{A_1^2 + B_1^2}}{A_1}\right]^{-1/2} \left[1 - \frac{4\Omega_d^2}{3\omega_d(\Delta\omega)}\right]^{-1/2} \quad (24)$$

$$v_{\phi-} \approx c\sqrt{2\Delta\omega} \left[\frac{-A_1 + \sqrt{A_1^2 + B_1^2}}{A_1}\right]^{-1/2} \times \left[\frac{A_1\omega_d^2}{\Omega_d\sqrt{A_1^2 + B_1^2}} + 2X \left(1 - \frac{2\Omega_d^2}{3\omega_d(\Delta\omega)}\right)\right]^{-1/2}. \quad (25)$$

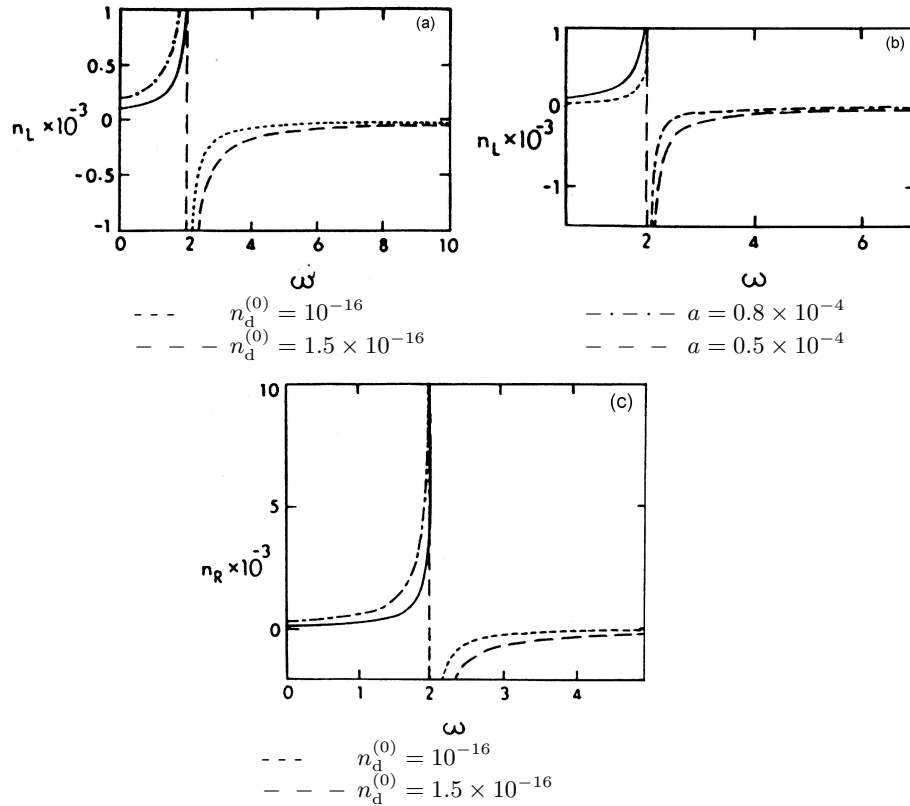


Figure 2. (a) Propagation of non-linear LCP waves: variation of n_L with frequency ω for $n_d^{(0)} = 10^{-16} \text{ cm}^{-3}$, $1.5 \times 10^{-16} \text{ cm}^{-3}$ (a fixed). (b) Propagation of non-linear LCP waves: variation of n_L with frequency ω for $a = 0.5 \times 10^{-4}$ stat volt/cm, 0.8×10^{-4} stat volt/cm (density fixed). (c) Propagation of non-linear RCP waves: variation of n_R with frequency ω for $n_d^{(0)} = 10^{-16} \text{ cm}^{-3}$, $1.5 \times 10^{-16} \text{ cm}^{-3}$ (a fixed).

The characteristics of the phase velocities for both LCP and RCP waves are as shown in figures 3a and 3b. From the figures it is clear that both the velocities decrease with the increase of ω in the domain $0 < \omega < \Omega_d$. Moreover, the phase velocity of the LCP wave has greater value than that of the RCP wave in the same frequency domain; e.g., for $\omega = 0.1$ rad/s, $v_{\phi+} \approx 10.5$ cm/s, $v_{\phi-} \approx 4.73$ cm/s. The numerical data taken correspond to Saturn's E-ring as mentioned earlier.

C. Group velocity

The non-linear group velocity expressions represented by $(d\omega/dk)$ for both LCP and RCP waves are obtained from (21) and (22) respectively as

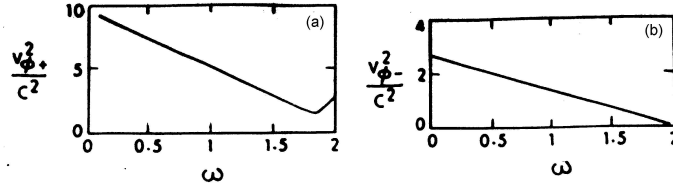


Figure 3. (a) $v_{\phi+}^2/c^2$ vs. ω diagram for LCP component of waves. (b) $v_{\phi-}^2/c^2$ vs. ω diagram for RCP component of waves.

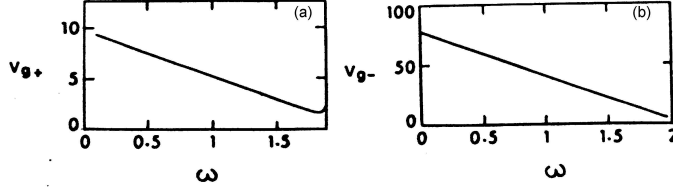


Figure 4. (a) v_{g+} vs. ω diagram for LCP component of waves. (b) v_{g-} vs. ω diagram for RCP component of waves.

$$1/v_{g+} \approx \frac{\Omega_d}{2c} \sqrt{\frac{X}{2}} \left[\frac{A_1 + \sqrt{A_1^2 + B_1^2}}{A_1} \right] \left[\frac{1}{(\Delta\omega)^{3/2}} - \frac{8\Omega_d^2}{3\omega_d(\Delta\omega)^{5/2}} \right] \quad (26)$$

$$\begin{aligned} 1/v_{g-} \approx & \frac{\omega_d}{2\sqrt{2}c} \left[\frac{\Omega_d(\sqrt{A_1^2 + B_1^2} - A_1)}{\sqrt{A_1^2 + B_1^2}} \right]^{1/2} \frac{1}{(\Delta\omega)^{3/2}} \\ & + \frac{\Omega_d^{3/2} X}{2c\omega_d A_1} \left(\sqrt{A_1^2 + B_1^2} - A_1 \right)^{1/2} (A_1^2 + B_1^2)^{1/4} \\ & \times \left[\frac{1}{\sqrt{2}(\Delta\omega)^{3/2}} - \frac{\sqrt{2}\Omega_d^2}{\omega_d(\Delta\omega)^{5/2}} \right]. \end{aligned} \quad (27)$$

The group velocity diagrams of the corresponding waves are shown in figures 4a and 4b. It is observed that the group velocity of the RCP wave is much larger than that of the LCP wave. Moreover, in both cases both the velocities decrease with the increase of frequency in the frequency domain $0 < \omega < \Omega_d$. For $\omega = 0.1$ rad/s, $v_{g+} \approx 9.26$ cm/s and $v_{g-} \approx 75.23$ cm/s.

D. Group travel time

The group travel time of propagation of a wave packet consisting of waves with frequency near Ω_d propagating along the path h is given by the integral (Gurnett *et al* [24])

$$t(\omega) = \int_0^h \frac{dh}{v_g}. \quad (28)$$

Using (26) and (27) in (28) we obtain the group travel time for LCP and RCP waves as

$$t(\omega)_+ \approx \frac{\Omega_d(o)}{c\Omega'_d(o)} \sqrt{\frac{X(o)}{2}} \left[\frac{A_1(o) + \sqrt{A_1^2(o) + B_1^2(o)}}{A_1(o)} \right] \times \left[\frac{1}{(\Delta\omega(o))^{1/2}} - \frac{8\Omega_d^2(o)}{9\omega_d(o)(\Delta\omega(o))^{3/2}} \right] \quad (29)$$

$$t(\omega)_- \approx \frac{\omega_d(o)}{2\sqrt{2}c\Omega'_d(o)} \left[\frac{\Omega_d(o)(\sqrt{A_1^2(o) + B_1^2(o)} - A_1(o))}{\sqrt{A_1^2(o) + B_1^2(o)}} \right]^{1/2} \frac{1}{(\Delta\omega(o))^{1/2}} + \frac{\Omega_d^{3/2}(o)X(o)}{c\Omega'_d(o)\omega_d(o)\sqrt{A_1(o)}} \left(\sqrt{A_1^2(o) + B_1^2(o)} - A_1(o) \right)^{1/2} \times (A_1^2(o) + B_1^2(o))^{1/4} \left[\frac{1}{\sqrt{2}(\Delta\omega(o))^{1/2}} - \frac{\sqrt{2}\Omega_d^2(o)}{3\omega_d(o)(\Delta\omega(o))^{5/2}} \right]. \quad (30)$$

Expressions (29) and (30) give the group travel times of the LCP and RCP waves with frequency near Ω_d from its origin to an observer (o). It is to be noted that in the absence of non-linearity, i.e., when $X(o) = 0$, expression (29) does not give the same whereas (30) leads to

$$t(\omega)_- \approx \frac{\omega_d(o)}{\sqrt{2}c\Omega'_d(o)} \left[\frac{\Omega_d(o) \left(\sqrt{A_1^2(o) + B_1^2(o)} - A_1(o) \right)}{\sqrt{A_1^2(o) + B_1^2(o)}} \right]^{1/2} \frac{1}{(\Delta\omega(o))^{1/2}}. \quad (31)$$

In the expressions (29)–(31) we have assumed the variation of density in the ionosphere to be small. Moreover, the cyclotron frequency $\Omega_d(h)$ is assumed to vary linearly in space; $\Omega_d(h) = \Omega_d(o) + h\Omega'_d(o)$, where $\Omega_d(o)$ is the cyclotron frequency at the observation point, and $\Omega'_d(o)$ the gradient of the cyclotron frequency.

For some quantitative estimation of group travel time, particularly to see the dependence of $t(\omega)_\pm$ on $\Omega'_d(o)$, density $n_d^{(0)}$ and amp. a , we have used the numerical data [21,24]. It is seen that for $\omega = 1.2 \times 10^{-5}$ rad/s, $t(\omega)$ varies from 36.43 s to 58.19 s as $\Omega'_d(o)$ varies from 0.5×10^{-3} rad/s/cm to 0.8×10^{-3} rad/s/cm for LCP wave and for RCP wave $t(\omega)$ varies from 6.32×10^{-11} s to 5.69×10^{-11} s as $\Omega'_d(o)$ varies from 0.3×10^{-3} rad/s/cm to 0.35×10^{-3} rad/s/cm. Thus the group travel time is increased by 60% with the increase of Ω'_d for LCP wave and for RCP wave the same is decreased by 10% with the increase of Ω'_d .

Moreover, we see that $t(\omega)$ also depends on the number density inside the plasma. Numerical estimation shows that for $\omega = 1.2 \times 10^{-5}$ rad/s and $\Omega'_d(o) = 0.3 \times 10^{-3}$ rad/s/cm, as n_i^0, n_d^0 vary from 20 to 25 cm^{-3} and 1.0 to 1.5 $\times 10^{-16}$ cm^{-3} , $t(\omega)$ varies from 21.86 s to 91.39 s for LCP wave, and for RCP wave this variation for $t(\omega)$ is from 6.32 to 8.2×10^{-11} s, i.e., in both cases $t(\omega)$ increases with the increase of number density inside the plasma. These variations are shown in figures 5a, 5b, 6b, 6c.

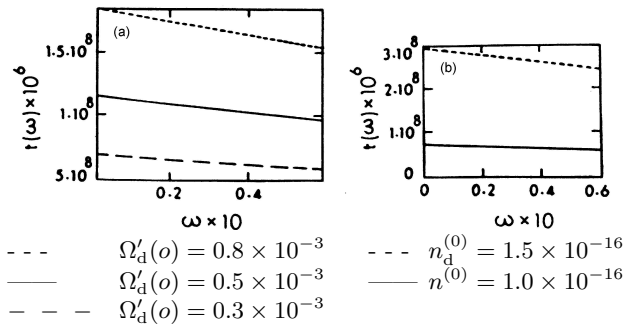


Figure 5. (a) Group travel time ($t(\omega)$) of LCP waves with the variation of frequency (ω) for $\Omega'_d(o) = 0.3 \times 10^{-3}$ rad/s/cm, 0.5×10^{-3} rad/s/cm, 0.8×10^{-3} rad/s/cm (density and amp. fixed). (b) Group travel time ($t(\omega)$) of LCP waves vs. frequency (ω) diagram for $n_d^{(0)} = 1.0 \times 10^{-16}$ cm $^{-3}$, 1.5×10^{-16} cm $^{-3}$ (frequency gradient and amp. fixed).

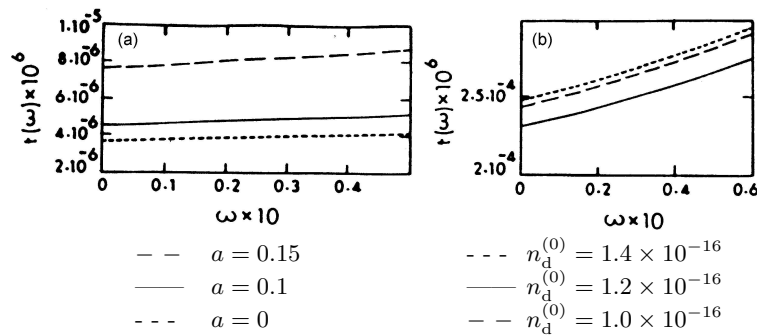


Figure 6. (a) Group travel time ($t(\omega)$) of RCP waves vs. frequency (ω) diagram for $a = 0.0, 0.1, 0.15$ stat volt/cm (frequency gradient and density fixed). (b) Group travel time ($t(\omega)$) of RCP waves vs. frequency (ω) diagram for $n_d^{(0)} = 1.0 \times 10^{-16}, 1.2 \times 10^{-16}, 1.4 \times 10^{-16}$ cm $^{-3}$ (frequency gradient and amp. fixed).

However, the variation of $t(\omega)$ for different values of the amp. for RCP wave is shown in figure 6a. The dependence of $t(\omega)$ for LCP wave on the amp. is clear from (34), i.e., as a increases $t(\omega)_+$ increases. Considering the variation of a from 0 to 0.1 stat volt/cm for a particular $\omega = 1.2 \times 10^{-5}$ c.p.s. we have observed from the numerical estimation that $t(\omega)$ varies from 1.43×10^{-13} s to 1.15×10^{-12} s.

E. Faraday rotation angle (FRA)

Due to the different dispersion rates of the LCP and RCP components of incident EM waves propagating along the external magnetic field \vec{B}_0 , the plane of polarisation undergoes a Faraday rotation through an angle given by

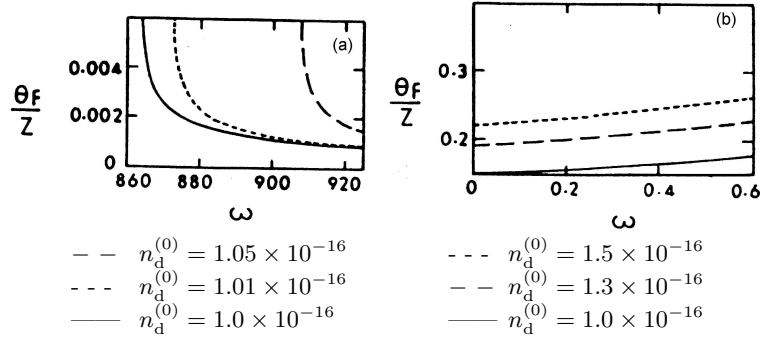


Figure 7. (a) Linear FRA vs. frequency diagram for $n_d^{(0)} = 1.0 \times 10^{-16} \text{ cm}^{-3}$, $1.01 \times 10^{-16} \text{ cm}^{-3}$, $1.05 \times 10^{-16} \text{ cm}^{-3}$. (b) Non-linear FRA vs. frequency diagram for $n_d^{(0)} = 1.0 \times 10^{-16} \text{ cm}^{-3}$, $1.3 \times 10^{-16} \text{ cm}^{-3}$, $1.5 \times 10^{-16} \text{ cm}^{-3}$.

$$\frac{\theta_F}{z} = \left(\frac{k_R - k_L}{2} \right),$$

where k_L, k_R are the wave numbers of RCP and LCP components and z the length. Therefore, in the presence of negatively charged dust grains, the linear and non-linear FRA are given by

$$\left(\frac{\theta_F}{z} \right)_{\text{linear}} \approx \frac{\Omega_d}{2c} \left[\left(1 - \frac{\omega_d^2}{\Omega_d(\omega - \Omega_d)} \right)^{1/2} - \left(1 - \frac{\omega_d^2}{\Omega_d(\omega + \Omega_d)} \right)^{1/2} \right] \quad (32)$$

$$\begin{aligned} \left(\frac{\theta_F}{z} \right)_{\text{non-linear}} &\approx \frac{\Omega_d}{2\sqrt{2}c(\Delta\omega)^{1/2}} \\ &\times \left(\frac{\omega_d^2(\sqrt{A_1^2 + B_1^2} - A_1)}{\Omega_d\sqrt{A_1^2 + B_1^2}} + \frac{2X(\sqrt{A_1^2 + B_1^2} - A_1)}{A_1} \right. \\ &\quad \left. - \frac{4X\Omega_d^2\sqrt{A_1^2 + B_1^2} - A_1}{3\omega_d\Delta\omega} \right)^{1/2} \\ &- \frac{\Omega_d}{2\sqrt{2}c(\Delta\omega)^{1/2}} \sqrt{\frac{X}{A_1}} \left(\sqrt{A_1^2 + B_1^2} + A_1 \right)^{1/2} \\ &\times \left(1 - \frac{4\Omega_d^2}{3\omega_d\Delta\omega} \right)^{1/2}. \end{aligned} \quad (33)$$

It is to be noted that though the non-linear FRA exists in the propagation band $0 < \omega < \Omega_d$, the linear FRA does not, rather it exists in $\omega > \frac{\omega_d^2}{\Omega_d} + \Omega_d$. Linear and non-linear FRA (figures 8a, 8b) for different values of ω in the propagation band with the variation of densities inside the plasma are shown in figures 7a, 7b. It is

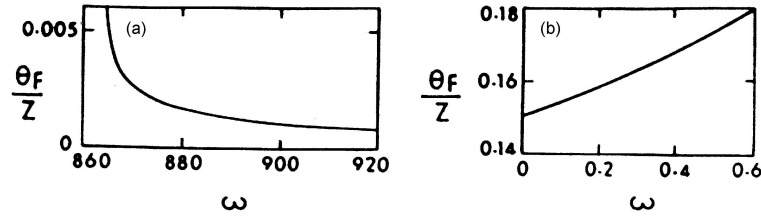


Figure 8. (a) Variation of linear FRA with frequency ω . (b) Variation of non-linear FRA with frequency ω .

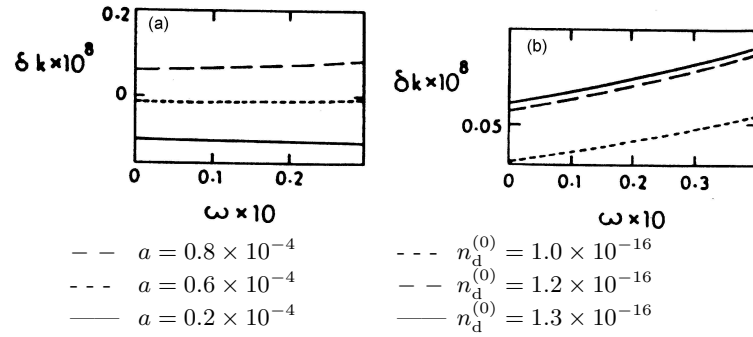


Figure 9. (a) Non-linear wave number shift vs. frequency diagram for $a = 0.2 \times 10^{-4}$ stat volt/cm, 0.6×10^{-4} stat volt/cm, 0.8×10^{-4} stat volt/cm (density fixed). (b) Non-linear wave number shift vs. frequency diagram for $n_d^{(0)} = 1.0 \times 10^{-16}$ cm $^{-3}$, 1.2×10^{-16} cm $^{-3}$, 1.3×10^{-16} cm $^{-3}$ (amp. fixed).

seen from the numerical estimation [21,24] that for a particular $\omega = 1.2 \times 10^{-5}$ rad/s as $n_e(0)$ and $n_d(0)$ vary from 1.0 to 0.7×10^{-1} cm $^{-3}$ and from 1.0 to 1.3×10^{-16} cm $^{-3}$ respectively, $(\frac{\theta_F}{z})_{\text{non-linear}}$ varies from 4.78 to 6.1×10^{-14} rad/s/cm. On the other hand $(\frac{\theta_F}{z})_{\text{linear}}$ varies from 0.9 to 2.2×10^{-15} rad/s/cm with the variation of $n_d^{(0)}$ from 1.0 to 1.01×10^{-16} cm $^{-3}$ for $\omega = 91.5$ rad/s in the domain $\omega > \frac{\omega_d^2}{\Omega_d} + \Omega_d$.

F. Non-linear wave number shift

Following Chakraborty and Paul [25] and Paul *et al* [26] we obtain the non-linear wave number shift of the waves with frequency near Ω_d . We substitute $K_+ = K + \delta k_+$ and $K_- = K + \delta k_-$ in eqs (21) and (22), where δk_{\pm} are the wave number shifts from their initial values K , with $|K| > |\delta k_{\pm}|$. Then neglecting the higher order terms occurring in δk_{\pm} we obtain

$$\delta k_+ \approx \frac{X\Omega_d (A_1 + \sqrt{A_1^2 + B_1^2})}{4cA_1(\Delta\omega)} \left(1 - \frac{4\Omega_d^2}{3\omega_d(\Delta\omega)} \right) \quad (34)$$

$$\delta k_- \approx \frac{\Omega_d^{3/2} \left(-A_1 + \sqrt{A_1^2 + B_1^2} \right)}{2c\omega_d A_1 (\Delta\omega)^{1/2}} \times \left[\frac{A_1 \omega_d^2}{\Omega_d \sqrt{A_1^2 + B_1^2}} + 2X \left(1 - \frac{2\Omega_d^2}{3\omega_d (\Delta\omega)} \right) \right] - \frac{\omega_d \sqrt{\Omega_d}}{2c(\Delta\omega)^{1/2}}. \quad (35)$$

Relations (34) and (35) clearly give the mutually complimentary non-linear wave number shifts for the LCP and RCP waves respectively. The average non-linear shift is given by

$$\delta k = \frac{1}{2} (\delta k_+ + \delta k_-), \quad (36)$$

where δk_{\pm} are given by (34) and (35). The variational effects of negatively charged dust grains as well as the nonlinear effects due to the presence of the intensity of the electric field on the estimate of the wave number shifts are shown in figures 9a, 9b. For numerical estimation we use the data [21,24] and see that for a particular $a = 0.8 \times 10^{-4}$ stat volt/cm, $\omega = 10^{-5}$ rad/s as $n_e^{(0)}$, $n_d^{(0)}$ vary from 1.0 to 0.8×10 cm $^{-3}$ and 1.0 to 1.2×10^{-16} cm $^{-3}$, $|\delta k|$ varies from 6.17 to 5.77×10^{-10} /cm and $k(\text{initial}) = \frac{1}{2}(k_+ + k_-)$ varies from 1451.42 to 1741.50/cm. Moreover, for $\omega = 10^{-5}$ rad/s, as a varies from 0.2 to 0.6×10^{-4} stat volt/cm, $|\delta k|$ varies from 9.91 to 1.33×10^{-10} /cm.

4. Conclusion

In our above analysis we have considered a low frequency transverse wave propagating through a magnetised dusty plasma with dust charge fluctuation and studied the propagation of the waves through the dispersion relation. Several important physical characteristics of the propagating waves, such as, phase velocity, group velocity, group travel time, Faraday rotation angle etc. are theoretically evaluated. It was shown that these parameters depend significantly on the amplitude of the wave as given by the non-linearity of the dispersion law. Also it was shown that the LCP and the RCP waves do differ in behaviours so far as the linearity and non-linearity are concerned. The charging processes of the dust grain also have important consequences on the mode of propagation. Finally, the graphical analysis of the non-linear dispersion relation explicitly gives the forbidden zone where the propagation is not possible. We have used a simplified model for dusty plasma. Dust particles are assumed to be spherical of definite size and mass. In fact, dust particles are of irregular sizes having different mass and charge. For more consistent treatment, the distribution of dust charge and size should be incorporated.

Acknowledgement

One of the authors (APM) wishes to thank CSIR (Govt. of India) for research fellowship. Valuable suggestions from the referee are gratefully acknowledged.

References

- [1] J M Dawson, *Phys. Rev.* **113**, 389 (1953)
- [2] F W Sluiter and D Montgomery, *Phys. Fluids* **8**, 551 (1965)
- [3] V N Tsytovich, *Nonlinear effects in plasma* (Plenum Press, New York, 1970)
- [4] B Chakraborty, S N Paul, M Khan and B Bhattacharya, *Phys. Rep.* **114**, 181 (1984)
- [5] C K Goertz, *Rev. Geophys.* **27**, 271 (1989)
- [6] N N Rao, P K Shukla and M Y Yu, *Planet Space Sci.* **38**, 543 (1990)
- [7] N F Cramer and S V Vledimirov, *Phys. Scr.* **53**, 586 (1996)
- [8] A C Breslin and K G Emeleus, *Phys. Lett.* **A31**, 23 (1970)
- [9] R N Carlile, S Gehe, J F O'Hanlon and J C Stewart, *Appl. Phys. Lett.* **59**, 1167 (1991)
- [10] M R Jana, A Sen and P K Kaw, *Phys. Rev.* **E48**, 3930 (1993)
- [11] R K Varma, P K Shukla and V Krishan, *Phys. Rev.* **E47**, 3612 (1993)
F Veerhest and P Meuris, *Phys. Lett.* **A210**, 198 (1996)
- [12] J X Ma and J Lin, *Phys. Plasma* **4**, 253 (1997)
- [13] A Barkman, R L Marlino and N D Angelo, *Phys. Plasma* **2**, 3563 (1995)
- [14] S Benkadda and V N Tsytovich, *Phys. Plasma* **5**, 1773 (1996)
- [15] A Roy Chowdhury, M K Alam and S N Paul, *Phys. Plasma* **6**, 3765 (1999)
- [16] S N Paul, K K Mondal and A Roy Chowdhury, *Phys. Lett.* **A257**, 165 (1999)
- [17] S Burman, S N Paul and A Roy Chowdhury, *Pramana – J. Phys.* **56**, 785 (2000)
- [18] K K Mondal, A Roy Chowdhury and S N Paul, *Phys. Rev.* **E65**, 0164 (2002)
- [19] F Verheest, *Waves in dusty space plasmas*, ISBN, 0-7923-6232-2
- [20] J R Bhat and B P Pandey, *Phys. Rev.* **E50**, 3980 (1995)
- [21] V N Tsytovich, G F Morfill, R Bingham and U de Angelis, *Comm. Plasma Phys. Controlled Fusion* **13(3)**, 153 (1990)
- [22] M Horayani, *Ann. Rev. Astron. Astrophys.* **34**, 383 (1996)
- [23] S Sarkar, B Chakraborty, M Khan and D Dutta, *Phys. Plasma* **3**, 468 (1996)
- [24] O A Gurnet, S D Shawan, N M Brice and R L Smith, *J. Geophys. Res.* **70**, 1665 (1965)
- [25] B Chakraborty and S N Paul, *Phys. Fluids* **26**, 2193 (1983)
- [26] S N Paul, A K Sur and G Pakira, *J. Plasma Phys.* **41**, 37 (1989)